Thermochimica Acta 685 (2020) 178540

Contents lists available at ScienceDirect

Thermochimica Acta

journal homepage: www.elsevier.com/locate/tca

An experimental approach based on inverse heat conduction analysis for thermal characterization of phase change materials

Swati Agarwala, K. Narayan Prabhu*

Department of Metallurgical and Materials Engineering, National Institute of Technology, Surathkal, Karnataka, India

ARTICLE INFO

Keywords:
Thermal energy storage
Inverse heat conduction problem
Solidification
Energy balance

ABSTRACT

A new method based on solution to inverse heat conduction problem for the assessment of solidification parameters of PCM salts has been proposed. The method estimates the mold -salt interfacial heat flux and it is used to calculate the latent heat of salt PCMs using calorimetry based energy balance equations. This method is more accurate compared to Computer Aided Cooling Curve Analysis (CACCA) techniques as it eliminates the drawbacks involved with base line fitting calculations and errors introduced due to the improper selection of solidification points. Pure salt PCMs such as KNO_3 and solar salt were used for the validation of this technique. Both air and furnace cooling were adopted to demonstrate the effect of cooling rate on solidification characteristics. The wettability of salt samples on mild steel surface was analyzed to account for the difference in the thermal behavior of salts.

1. Introduction

The development and growth of the renewable source of energy is increasing and is expected to increase further in the near future. Solar energy is an important source of this renewable energy. The only drawback associated with it is its intermittent nature. In order to create a continuous and reliable stream of power throughout without interruption, there is a need to store this excess thermal energy. Energy storage integrated with solar thermal power generation will help in the reduction of pollution and hence global warming. This thermal energy storage systems (TES) are of two types, sensible heat thermal energy storage systems (SHTES) and latent heat thermal energy storage systems (LHTES). The LHTES using phase change materials (PCMs) is considered to more promising than SHTES due to its higher energy storage density particularly at constant temperature or narrow temperature range [1].

For successful development and implementation of the PCMs, an accurate database of the various solidification parameters and thermophysical properties of these materials is very important which can be obtained by the thermal characterization of these PCMs. Thermal analysis is a reliable technique which is used for characterization of the energy storage materials. In this technique, the temperature dependent properties are measured. Differential scanning calorimetry (DSC) is the technique widely used by researchers to measure solidification parameters and the thermophysical properties. However, the limitation on the sample size has restricted its usage. In the case of inhomogeneous samples, the DSC results are reflective of the sample used, not of the entire material used. Another limitation associated with DSC is the loss of latent heat due to overestimation of the super cooling. The results obtained are affected by the rates of heating and cooling used which also affects the measured values. Due to these limitations, researchers are looking for alternate characterization techniques. T-history method is an alternate calorimetry based thermal characterization method. This technique incorporates larger sample size unlike DSC. Here reference materials are needed for the analysis of PCMs. Many researchers have used this technique for low temperature applications especially organic PCMs. However, the reference material and dimensional constraint; limits its usage for high temperature applications. Because of such limitations, a new method called as computer aided cooling curve analysis (CACCA), based on the analysis of the thermal behavior and the cooling rate curve is widely used. This CACCA method can be used to evaluate the solidification characteristics and the latent heat of the PCMs during solidification [2].

Newtonian and the Fourier methods are the two characterization techniques which uses CACCA technique as their basis and have gained importance among researchers in recent times. In both these methods, the PCMs are characterized only during the cooling cycle. The Newtonian technique is a one thermocouple system whereas the Fourier is a two thermocouple system. The Fourier technique takes the thermal gradient obtained within the salt sample into consideration. Both these

* Corresponding author.
E-mail addresses: s.agarwala16@gmail.com (S. Agarwala), prabhukn_2002@yahoo.co.in (K.N. Prabhu).

https://doi.org/10.1016/j.tca.2020.178540
Received 27 November 2019; Received in revised form 30 January 2020; Accepted 31 January 2020
Available online 02 February 2020
0040-6031/

Nomenclature

A	Heat transfer area (m^2)
B(t)	Temperature distribution at the outer surface of the mold
c_p	Specific heat capacity (J/kgK)
dT /dt	Cooling rate (°C/s)
dT /dr	Thermal gradient in the radial direction
g	Acceleration due to gravity (m/s^2)
Gr	Grashof number
h	Heat transfer coefficient (W/m^2K)
H	Phase change enthalpy/latent heat (J/kg)
k	Thermal conductivity (W/mK)
k_f	Thermal conductivity of air at room temperature (W/mK)
l	Iteration number
L	Thickness of the mold (m)
L_1	Position of the T3 thermocouple (2mm from the salt/mold interface)
L	Characteristic length of the cylinder (m)
m	Sample mass (kg)
Nu	Nusselt number
Pr	Prandtl number
q	Heat flux (W/m^2)
q_{M+1}	Heat flux at any future time step (W/m^2)
Q	Net heat liberated from the sample into the mold (W)
Q_{inst}	The rate of heat liberated during solidification (W)
Q_{total}	Total heat liberated during the phase change (J)
r	Inner radius of the mold (m)
r	Number of future time temperature +1
t	Time (s)
t_e	Time corresponding to the temperature T_s-5
t_s	Time corresponding to the temperature T_l+5
T_0	Ambient temperature (°C)
Ti	Initial temperature (°C)
T_{n+i}	Calculated temperature at a particular time step (°C)
T_s	End of solidification point
T_l	Start of solidification point
Ts	Surface temperature (°C)
T∞	Bulk temperature (°C)
Y(t)	Measured thermocouple temperature at L1 position
Y_{n+i}	Measured temperature at a particular time step (°C)
β	Coefficient of thermal expansion (1/K)
Δθ	Time step for heat flux
Δt	Time step for temperature
ε	A very small value
ν	Kinematic viscosity (m^2/s)
ρ	Density (kg/m^3)
φ	Sensitivity coefficient

techniques involve the calculation of the zero curve or an imaginary curve also called as baseline. These baseline calculations involve linear fitting and appropriate selection of the start and end points of solidification. The results obtained here are very much affected by the fitting techniques and the choice of the solidification points which serve as a major source of error in the calculated values.

In the present work, the thermal characterization of the chosen salts is done by estimating the metal/salt interfacial heat flux by solving one dimensional Fourier heat conduction problem inversely. Inverse heat conduction problem (IHCP) estimates the boundary conditions of a sample where the thermal history within the sample is known unlike direct heat conduction problem where the thermal history within the sample is calculated using the known boundary conditions. IHCP can be used in wide range of applications in the field of material processing, solidification and quenching. In the case of solidification processing, the heat removed from the casting can be estimated by knowing the heat transfer at the casting/mold interface. This interfacial heat flux can be estimated using IHCP. The solidification characteristics of the casting/mold and casting/chill can be estimated using IHCP. Another area where IHCP has been found useful is in estimation of the cooling characteristics of the quench medium during quench hardening. IHCP is used for the estimation of heat flux at the metal/quenchant surface during various stages of quenching. The estimated heat flux quantifies the cooling performance of the quench medium. The implementation of IHCP in thermal characterization of phase change materials is adopted in the present work where the heat flux at the salt/mold interface is estimated [3].

Using simple energy conservation equations, solidification parameters and the phase change enthalpy are determined. A pure salt KNO_3 and solar salt (60 wt% $NaNO_3$ and 40 wt% KNO_3) were used for the validation of this method.

2. Materials and methods

2.1. Experimental setup and devices

The IHCP-energy balance technique using graphite crucible explained in [4] had certain limitations related to the graphite crucible used in the experimental method.

(1) The durability of the crucible was a concern due to frequent cracking during experiments.
(2) The loss of molten salt sample and absorption of moisture due to the porous nature of the crucible material.
(3) The literature presents a wide range of thermophysical properties for graphite. The selection of inappropriate thermophysical properties can induce errors in the results of the heat flux data obtained.
(4) The retention of the salt sample in the crucible which prevents the reuse of the crucible.

To overcome the above limitations, a steel mold as shown in Fig. 1 was used in this work.

The salt sample was melted in a steel mold with O.D. 50 mm, I.D. 20 mm and height 125 mm and L/D ratio greater than 5. The top and bottom of the mold was thermally insulated by using a layer of ceramblanket. The average specific heat capacity of salt samples used in the present work are given in Table 1. The mass of the steel mold was 1.731 kg. Mass of KNO_3 and solar salt used was 0.058 kg and 0.065 kg respectively.

Three inconel sheathed K-type thermocouples of 1 mm diameter were used in this method. One thermocouple T1 was placed at the center of the sample while two thermocouples were placed in the mold itself. T2 thermocouple was placed at a distance of 2 mm from the outer surface of the mold. Another thermocouple T3 was placed at a distance of 2 mm from the inner surface of the mold. The temperature data was acquired at a scanning frequency of 2 Hz. For data processing NI USB 9213 data acquisition system was used. The schematic sketch of the set up used for the experimentation is shown in Fig. 2.

2.2. Experimental methodology

The estimation of the heat flux transients at the interface of salt and the mold was done using TmmFe Inverse solver (Thermet solutions, Pvt. Ltd., Bangalore). In inverse heat conduction problem, the interfacial heat flux is estimated by the use of Beck's nonlinear estimation technique. The one dimensional heat conduction equation (Eq. 1) in cylindrical coordinates is solved using the boundary and initial conditions.

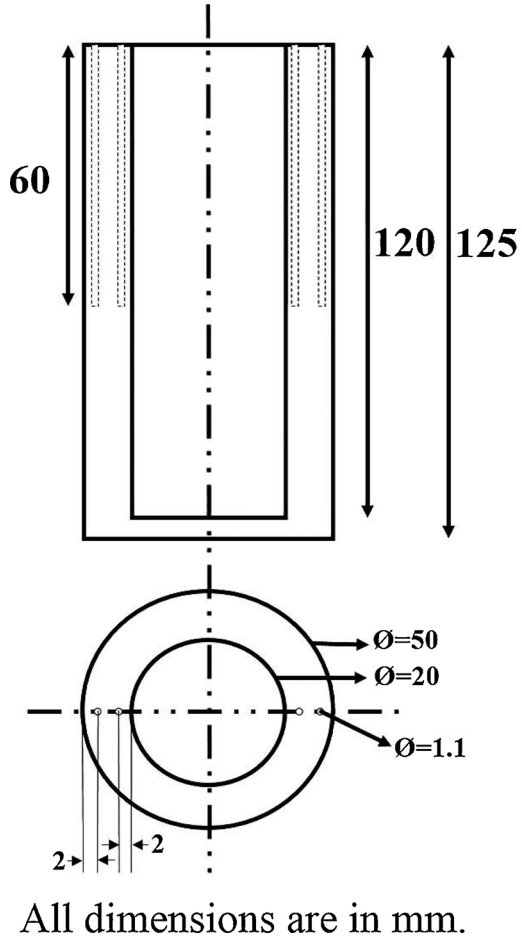

Fig. 1. Schematic model of the steel mold.

Table 1
Average specific heat capacity values of the salts.

Materials	Average specific heat capacity (kJ/kg K)
KNO_3	1.20 [5]
60 wt% $NaNO_3$ and 40 wt% KNO_3 (Solar salt)	1.485 [6]

$$\frac{1}{r}\frac{\partial}{\partial r}\left(kr\frac{\partial T}{\partial r}\right) = \rho C_p \frac{\partial T}{\partial t} \tag{1}$$

The boundary and initial conditions used were:

T (L_1, t) = Y (t) (Measured thermocouple temperature (T3) at a distance of L_1 = 0.002 m from the interface)

T (L, t) = B (t) (Thermal boundary condition at the outer surface of the mold)

T (L, 0) = Ti (Initial temperature)

where L is the thickness of the mold model

To determine the heat flux at L = 0, i.e. at the interface, the following error function 'F (q)' has to be minimum.

$$F(q) = \left(\sum_{i=1}^{I=mr} (T_{n+i} - Y_{n+i})^2\right) \tag{2}$$

Where r = number of future time temperature +1 and $m = \Delta\theta/\Delta t$ where $\Delta\theta$ and Δt are the time steps for heat flux and temperature respectively and T_{n+i} and Y_{n+i} are the calculated and measured temperatures at the thermocouple (T3) position.

The main objective here is to calculate q_{M+1} using present and future temperatures. The future temperatures are calculated at higher time steps than the present temperatures. The key assumption here is that the $q_{M+2} = q_{M+3} = q_{M+r} = q_{M+1}$ which means q is constant over the future time steps. For the l^{th} iteration the Taylor series expansion for future temperature was used and is given by:

$$T_{n+i}^{l} \approx T_{n+i}^{l-1} + \frac{\partial T_{n+i}^{l-1}}{\partial q_{M+1}^{l}}(q_{M+1}^{l} - q_{M+1}^{l-1}) \tag{3}$$

For the start of the 1^{st} iteration q value can be assumed as unity. This partial derivative in the Eq. (3) is the sensitivity coefficient (∅) which is defined as the temperature change with respect to a small change in the heat flux at the surface.

$$\varnothing_i^{l-1} = \frac{T_{n+i}(q_{M+1}^{l-1}(1+\varepsilon)) - T_{n+i}(q_{M+1}^{l-1})}{\varepsilon q_{M+1}^{l-1}} \tag{4}$$

The numerator in the above equation corresponds to the change in temperature when the heat flux q increased by a small value which is q + εq.

To evaluate the increment in heat flux for the next iteration the error function with respect to heat flux should be minimum therefore,

$$\frac{\partial F(q)}{\partial q} = 0 \tag{5}$$

So, substituting the error function as shown in Eq. 2 in Eq. 5,

$$\frac{\partial}{\partial q}\left(\sum_{i=1}^{I=mr} (T_{n+i} - Y_{n+i})^2\right) = 0 \tag{6}$$

Substituting Eq. 3 in Eq. 6,

$$\frac{\partial}{\partial q}\left(\sum_{i=1}^{I} (T_{n+i}^{l-1} + \varnothing_i^{l-1}(q_{M+1}^{l} - q_{M+1}^{l-1}) - Y_{n+i})^2\right) = 0 \tag{7}$$

Which gives,

$$\sum_{i=1}^{I} \varnothing_i^{l-1}(T_{n+i}^{l-1} - Y_{n+i} + \varnothing_i^{l-1}(\nabla q_{M+1}^{l})) = 0 \tag{8}$$

After rearranging the Eq. 8,

$$\nabla q_{M+1}^{l} = \frac{\sum_{i=1}^{I}(Y_{n+i} - T_{n+i}^{l-1})\varnothing_i^{l-1}}{\sum_{i=1}^{I}(\varnothing_i^{l-1})^2} \tag{9}$$

Where,

$$\nabla q_{M+1}^{l} = q_{M+1}^{l} - q_{M+1}^{l-1} \tag{10}$$

This procedure is repeated till we get a new heat flux value and the following condition is satisfied.

$$\frac{\nabla q_{M+1}^{l}}{q_{M+1}^{l-1}} < 0.005 \tag{11}$$

If the condition in Eq. 11 is satisfied then the heat flux value obtained will be taken as the heat flux for the next time step or else it will be the input for the next iteration and the whole process will be again repeated [3,7]. A flowchart depicting the inverse heat conduction problem is shown below in Fig. 3 for clear understanding.

2.3. Experimental technique

Salts KNO_3 and $NaNO_3$ were procured from Molychem Pvt. Ltd, Mumbai. KNO_3 was used as it is for the experiments. The solar salt was prepared by taking 60 wt % $NaNO_3$ and 40 wt % of KNO_3 in a stainless steel container. It was then heated in a resistance furnace at a temperature of 300 °C to ensure complete melting of salts. After this, it was transferred to a muffle furnace maintained at a temperature of 250 °C for 2 days to ensure complete homogenization of the salt mixture. The salt thus obtained was used as solar salt during experimentation.

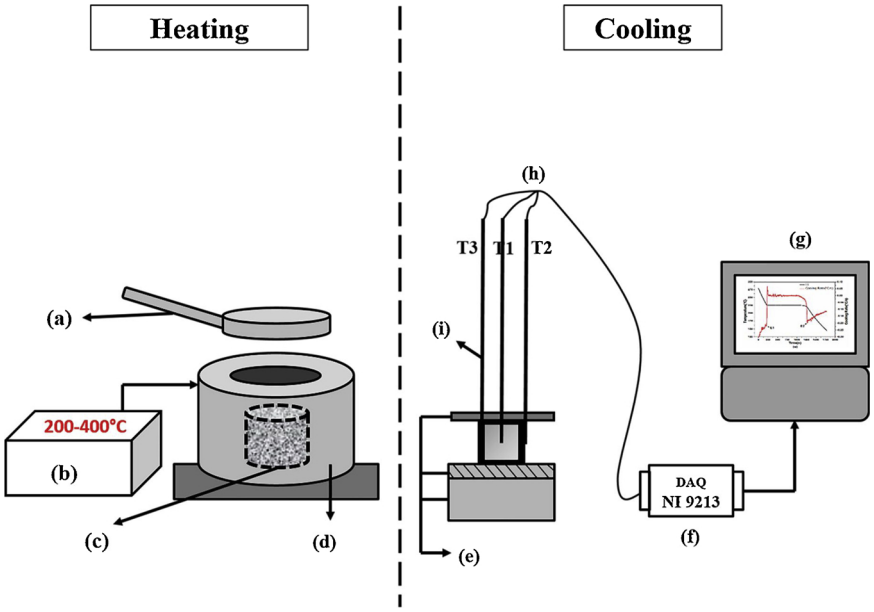

Fig. 2. Schematic drawing illustrating the used Experimental setup (a) Furnace lid (b) Furnace controller (c) Steel mold with the sample material (d) Temperature controlled resistance furnace (e) Insulation (f) Data acquisition system (g) PC monitor (h) Connecting cables (i) K-type thermocouples.

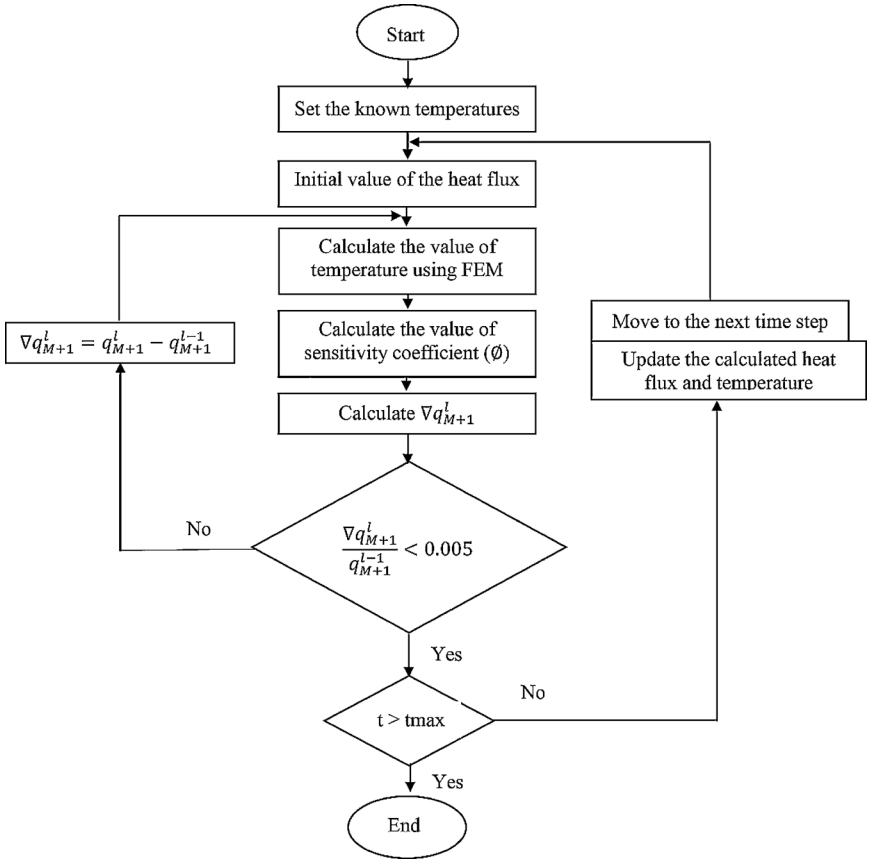

Fig. 3. Flow chart representing the methodology of the inverse heat conduction algorithm.

For experiments, the salt sample was taken in the steel mold and melted using resistance furnace. For air cooling experiments, the mold with the molten salt was taken out of the furnace and kept in the ambient environment. While, in the case of furnace cooling the mould was cooled in the furnace itself. During cooling the thermocouples were employed to record the thermal history of salt and cooling of the mold near to the inner and outer surface.

The temperature data close to the inner surface of the mold (T3) and the thermophysical properties of the steel mold were used as input to the Tmmfe solver. To represent the steel mold, a model with cylindrical axi-symmetry was used in the inverse solver with a four node quadrilateral element. The mesh size used in the axisymmetric model 30 × 30 with 900 elements for air cooling and 4 × 30 with 120 elements for furnace cooling. The convergence limit used during the

Table 2
Boundary Conditions of Air cooled and Furnace cooled steel mold.

Boundaries	Air cooled	Furnace cooled
R1	Unknown heat flux "q"	Unknown heat flux "q"
R2 and R3	q = 0, insulated	q = 0, insulated
R4	h = 10 W/m^{2}K,T$_o$ = Ambient temperature (°C)	Thermal boundary using T2 thermocouple data

inverse simulation was 1E-6. Two sets of experiments based on air and furnace cooling were performed. The boundary conditions in both cases are shown in Table 2.

The boundary condition of h = 10 W/m^{2}K for air cooling was taken from the literature [8] under the condition of free convection over a vertical cylinder. The heat transfer coefficient was estimated using Nusselt number (Nu) where, Nusselt number is given by the Eq. 12.

$$Nu = \frac{hL}{k_f} \tag{12}$$

where, h is the heat transfer coefficient (W/m^{2}K), L = characteristic length of the cylinder (m) and k_f is the thermal conductivity of air at room temperature (W/mK). Nusselt number for laminar flow with free convection over a vertical cylinder is given by Eq. 13

$$Nu = 0.59(Gr \times \Pr)^{0.25} \tag{13}$$

where, Gr is the Grashof number and Pr is the Prandtl number. Grashofs number is given by the Eq. 14.

$$Gr = \frac{g\beta(Ts - T\infty)L^3}{\nu^2} \tag{14}$$

All the thermophysical properties are of air and Prandtl number is of air at room temperature which is 0.7282.

A schematic representation of the inverse solver model of the steel mold used for the approximation of the heat flux is shown in Fig. 4.

Using the estimated heat flux (q) data obtained from the inverse solver, the net heat liberated from the sample into the mold (Q) was determined by multiplying the heat flux (q) with the heat transfer area (A).The energy balance Eq. (15) was employed at the inner surface of the mold and the rate of heat liberated at each time interval during the phase change (Q_{inst}) was calculated.

$$Q_{inst} = q \times A - m \times c_p \times \frac{dT}{dt} \tag{15}$$

The rate of heat liberated during solidification (Q_{inst}) was integrated over the solidifying range to obtain the total heat liberated during the phase change (Q_{total}). During the calculation of Q_{total} for KNO_3, the area under the curve in the artificial solidification range was considered as the interfacial heat flux curve did not significantly reflect the phase transformation of the salt. In the solar salt sample, the solidification of the salt was significantly reflected on the heat flux curve at the mold /salt interface. Therefore for solar salt, the absolute area under the curve with end points of solidification as baseline was considered for the estimation of Q_{total} as per Eq. 16. This Q_{total} was divided by the mass of the sample to obtain the phase change enthalpy per unit mass (H) as per the Eq. 17.

$$Q_{total} = \int_{t_e}^{t_s} Q_{inst} \tag{16}$$

$$H = \frac{Q_{total}}{m} \tag{17}$$

Where, ts and te represents the time corresponding to the temperatures $T_l + 5$ and T_s-5 respectively, m = sample mass (kg), A = heat transfer area (m^2), c_p = Average specific heat of the salt (J/kgK), dT/dt = cooling rate (°C/sec) and H = phase change enthalpy/latent heat (J/kg).

The major source of error while determining the latent heat is the choice of a start and end temperature of solidification used for integrating the heat flow peak (Q_{inst}). To alleviate this problem, an artificial mushy zone with an initial temperature of 5 °C before the start of solidification temperature (T_l) and 5 °C after the end of solidification temperature (T_s) was chosen.

The T2 thermocouple data is used to calculate the error between the estimated and measured temperature at 2 mm from the outer surface of the mold where T2 thermocouple was placed. This will help to check the reliability of the estimated heat flux and also help in the validating the boundary condition used. The error was calculated using Eq. 18.

$$Error\% = \left(\frac{T_{measured} - T_{estimated}}{T_{measured}}\right) \times 100 \tag{18}$$

The % error estimated for KNO_3 and solar salt were 0.4 and 0.02

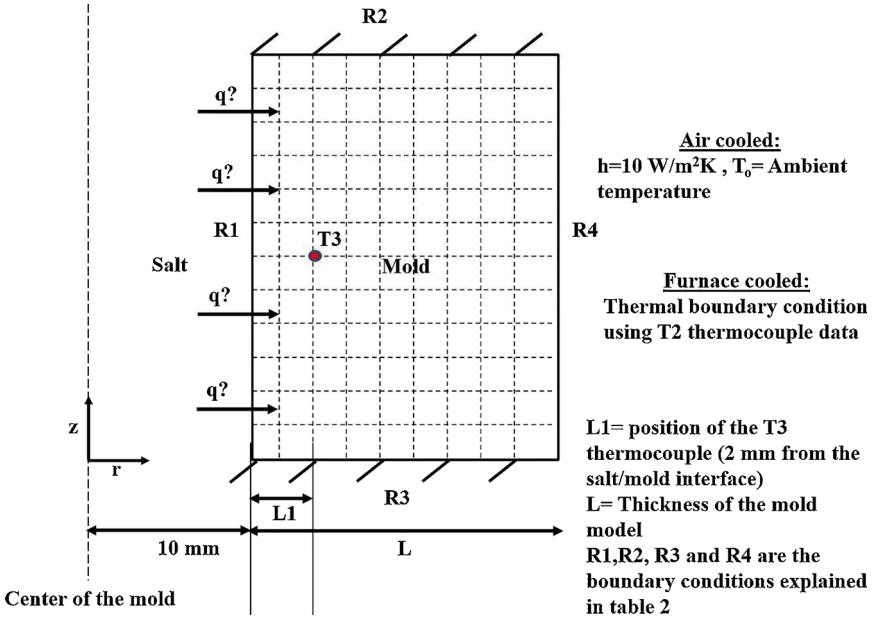

Fig. 4. Schematic drawing illustrating the inverse solver model of the steel mold.

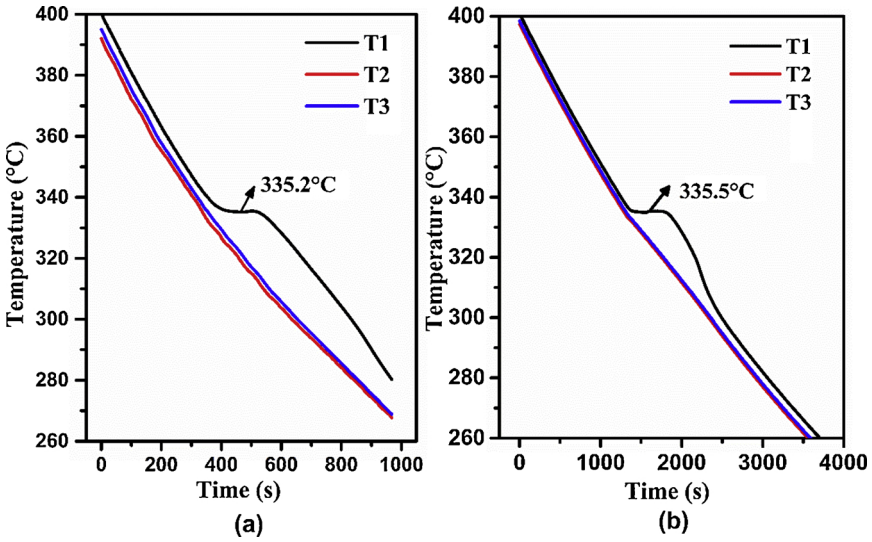

Fig. 5. Thermal history obtained with KNO_3 and steel mold (a) Air cooled (b) furnace cooled.

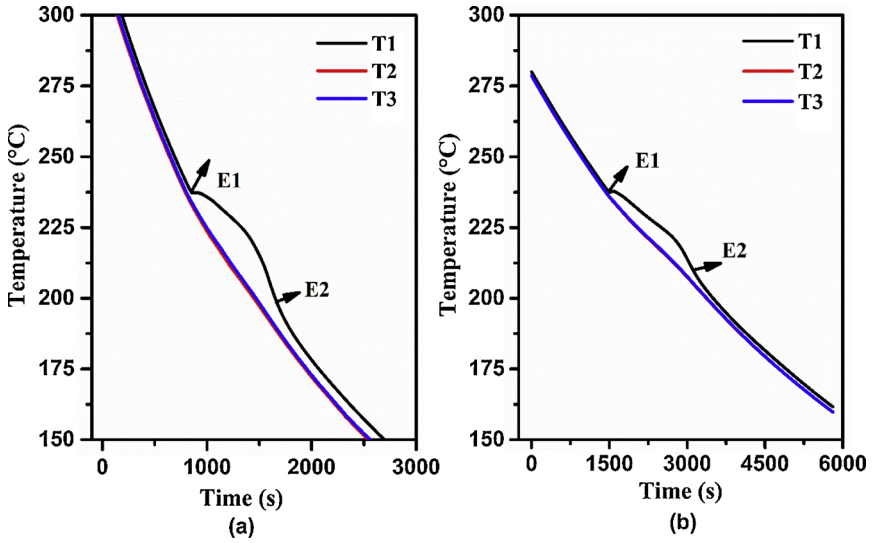

Fig. 6. Thermal history obtained with 60 wt% $NaNO_3$ and 40 wt% KNO_3 solar salt and steel mold (a) Air cooled (b) furnace cooled.

respectively. This shows that the difference between the measured and estimated temperatures was significantly less and therefore the heat flux obtained and chosen boundary conditions were quite reliable.

The wettability of the salts was studied on a polished mild steel surface using the Drop shape analyzer (DSA100, Kruss, Germany). The contact angle of the salts was measured and tabulated.

3. Results and discussion

The solidification process of KNO_3 and the solar salt along with the cooling history of the mold in both cases of air and furnace cooling is shown in Figs. 5 and 6 where T1, T2 and T3 represent the center thermocouple data and the temperature data near to the outer and inner surface of the mold respectively.

In the case of air cooled KNO_3, as per the solidification process shown in Fig. 5, the salt changes its phase at a temperature of 335.2 °C representing its melting temperature. KNO_3 took 229 s for complete phase change considering the ± 5 range. In the case of furnace cooling, the temperature of the phase change was 335.5 °C and the salt took 711 s for its solidification.

For solar salt, considering the ± 5 range, the solidification starts at 242 °C and ends at 205 °C for both the cooling processes. The total time taken for solidification is 817 s and 1993.5 s for air cooling and furnace cooling respectively as shown in the Fig. 6.

The cooling rate curve was superimposed on the cooling curve of KNO_3 and 60 wt% $NaNO_3$ and 40 wt% KNO_3 solar salt as shown in Figs. 7 and 8.

It can also be observed that the cooling rate had no significant effect on the phase change parameters of the salt samples.

The estimated heat flux at the interface of the salt and the mold for KNO_3 and 60 wt% $NaNO_3$ and 40 wt% KNO_3 solar salt are shown in Figs. 9 and 10.

A drop in the heat flux curve in the solidification range was observed for solar salt as shown in Fig. 10 which was due to the phase transformation of the salt. Such a drop was not significantly observed in KNO_3 heat flux data.

The phase change enthalpy values for KNO_3 in this method was calculated to be 88.85 kJ/kg and 108.9 kJ/kg during air cooling and furnace cooling respectively while the reported literature values are 91 kJ/kg and 102 kJ/kg [5,9] It can be observed that the latent heat values obtained using this method were nearly close to the reported values of literature.

The phase change enthalpy calculated using this method for the solar salt was 92 kJ/kg and 104.1 kJ/kg for air cooling and furnace

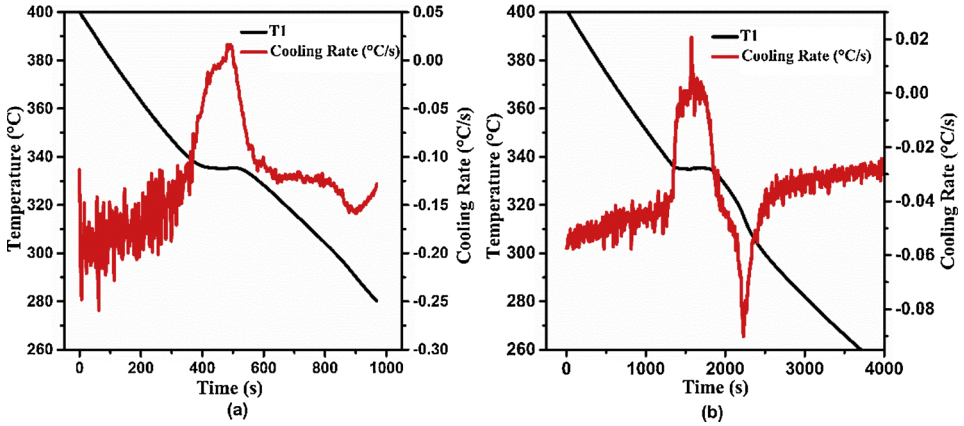

Fig. 7. The cooling curve and the cooling rate curves of KNO_3 (a) Air cooled (b) furnace cooled.

cooling respectively. The values calculated were in agreement with the data reported (98 kJ/kg) in literature [10].

The wetting behavior of the salts on the mild steel surface is shown in Fig. 11.

The contact angle between the salt and the steel surface is measured and given in Table 3.

From the wetting behavior as shown in Fig. 11 and contact angle analysis data as shown in Table 3, it was observed that the contact angle of the solar salt on the mild steel surface was lower than KNO_3 indicating better wettability of solar salt. The lower wettability of KNO_3 on mild steel surface leads to the formation of air pockets at the interface which acts as a barrier to the heat transfer from the salt to the mold. Therefore the salt/ mold interfacial heat flux data did not capture the phase transformation during solidification of the salt. However in the case of solar salt, the wetting tendency is higher leading to a conforming contact at the salt/ mold interface and lower resistance to interfacial heat transfer. Therefore the heat flux transients clearly reflect the phase transformation of the solar salt as indicated by a sharp drop during the solidification range.

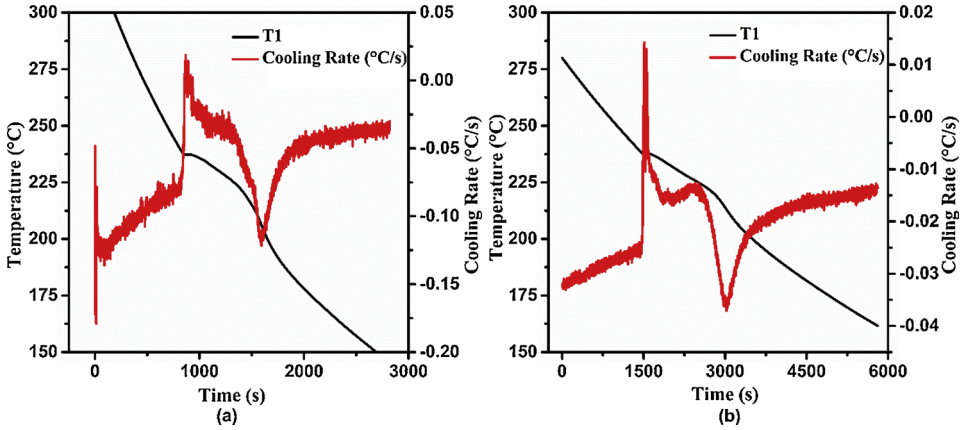

Fig. 8. The cooling curve and the cooling rate curves of 60 wt% $NaNO_3$ and 40 wt% KNO_3 solar salt (a) Air cooled (b) furnace cooled.

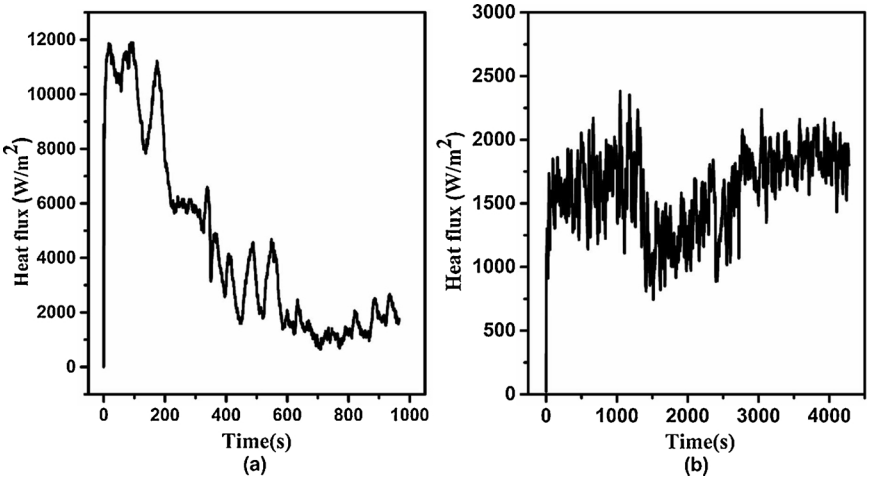

Fig. 9. Estimated heat flux transients for the salt KNO_3 (a) Air cooled (b) furnace cooled.

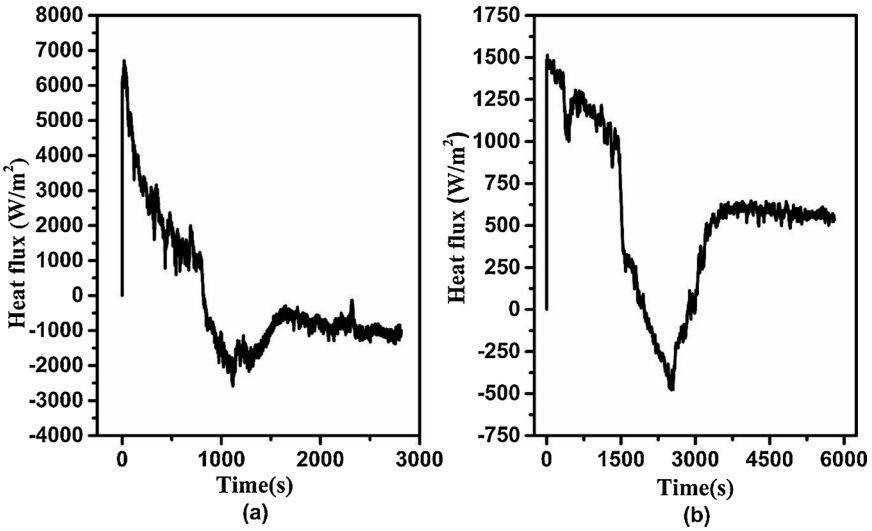

Fig. 10. Estimated heat flux transients for the 60 wt% $NaNO_3$ and 40 wt% KNO_3 solar salt (a) Air cooled (b) furnace cooled.

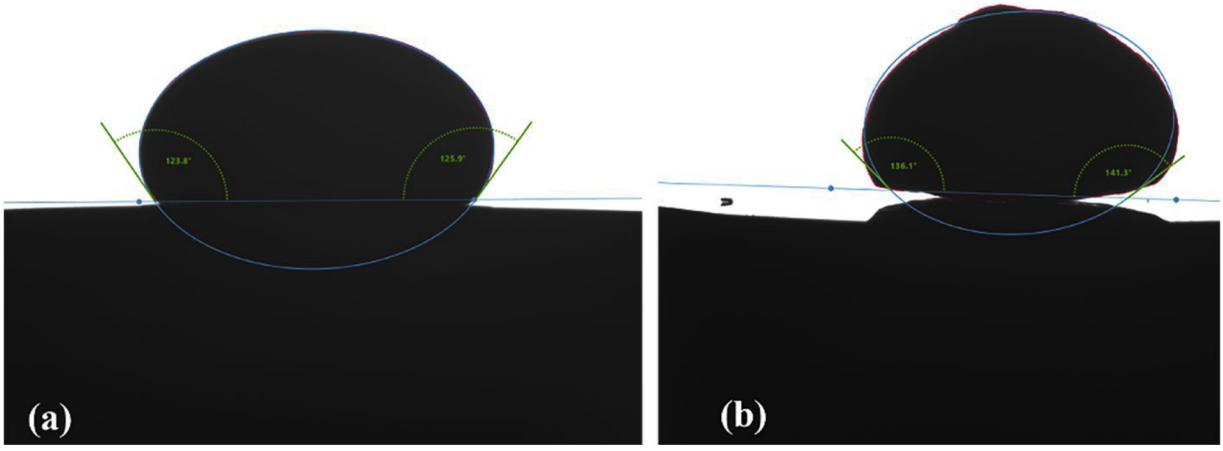

Fig. 11. Wetting behavior of the salt samples on the mild steel surface (a) solar salt (b) KNO_3 salt.

Table 3
Contact angle data for both the salt samples on the mild steel surface.

Salt sample	Mean contact angle	Contact angle(left)	Contact angle(right)
Solar salt	124.88°	123.8°	125.9°
KNO_3	138.69°	136.1°	141.3°

4. Conclusion

The method based on solution to inverse heat conduction eliminates all the limitations associated with the conventional characterization techniques. The method involves no baseline calculations and thus error associated with it is avoided. To alleviate the issue of choosing the initial and final temperature of solidification, an initial temperature of Tl + 5 and final temperature of Ts-5 was chosen in this method. The phase change parameters and the calculated latent heat values of the KNO_3 and solar salt samples using this modified method were found to be in good agreement with the reported literature data.

This study also incorporates the effect of both air cooling and furnace cooling of salt samples in the steel mold and it was observed that the cooling rate has no significant effect on the solidification characteristics of salt samples. Wetting behavior of the salts on the mild steel surface were assessed. The wettability of the solar salt was higher than KNO_3. The solar salt with good contact at the interface would offer lower resistance to heat transfer whereas KNO_3 would offer more resistance to heat flow due to the non-conforming interfacial contact. The results obtained from this work show that the modified IHCP-energy balance method is very promising for thermal characterization of salt based phase change materials.

CRediT authorship contribution statement

Swati Agarwala: Conceptualization, Methodology, Data curation, Validation, Investigation, Writing - original draft. **K. Narayan Prabhu:** Supervision, Conceptualization, Writing - review & editing.

References

[1] A. Sharma, V.V. Tyagi, C.R. Chen, D. Buddhi, Review on thermal energy storage with phase change materials and applications, Renewable Sustainable Energy Rev. 13 (2) (2009) 318–345, https://doi.org/10.1016/j.rser.2007.10.005.
[2] H. Mehling, L.F. Cabeza, Heat and Cold Storage With PCM: an up to Date Introduction Into Basics and Applications, Verlag Berlin Heidelberg, springer, 2008.
[3] K. Narayan Prabhu, A.A. Ashish, Inverse modeling of heat transfer with application to solidification and quenching, Mater. Manuf. Process. (2002) 469–481, https://doi.org/10.1081/AMP-120014230.
[4] S. Agarwala, K.N. Prabhu, Assessment of solidification parameters of salts and metals for thermal energy storage applications using IHCP-Energy balance combined technique, Trans. Indian Inst. Met. 71 (11) (2018) 2677–2680, https://doi.org/10.1007/s12666-018-1407-8.
[5] R. Sudheer, K.N. Prabhu, A Computer aided Cooling Curve Analysis method to study phase change materials for thermal energy storage applications, Mater. Des.

95 (2016) 198–203, https://doi.org/10.1016/j.matdes.2016.01.053.
[6] G. Cáceres, K. Fullenkamp, M. Montané, K. Naplocha, A. Dmitruk, Encapsulatednitrates phase change material selection for use as thermal storage and heat transfer materials at high temperature in concentrated solar power plants, Energies. 10 (2017), https://doi.org/10.3390/en10091318.
[7] L. Zhang, C. Reilly, L. Li, S. Cockcroft, L. Yao, Development of an inverse heat conduction model and its application to determination of heat transfer coefficient during casting solidification, Heat Mass Transf. 50 (2014) 945–955, https://doi.org/10.1007/s00231-014-1304-6.
[8] D.R. Poirier, G.H. Geiger, Transport Phenomena in Materials Processing, Minerals, Metals & Materials Society, Warrendale, Pa, 1994.
[9] F. Roget, C. Favotto, J. Rogez, Study of the KNO_3-$LiNO_3$ and KNO_3-$NaNO_3$ $LiNO_3$ eutectics as phase change materials for thermal storage in a low-temperature solar power plant, Sol. Energy 95 (2013) 155–169, https://doi.org/10.1016/j.solener.2013.06.008.
[10] M. Lasfargues, Q. Geng, H. Cao, Y. Ding, Mechanical dispersion of nanoparticles and its effect on the specific heat capacity of impure binary nitrate salt mixtures, Nanomaterials 5 (2015) 1136–1146, https://doi.org/10.3390/nano5031136.